solid angle subtended by N (4.8% of the sphere) was not small, events in which more than one secondary would intercept N were tabulated separately in the Monte-Carlo calculation. The detection probability for these events was obtained from the appropriate combination of detection probabilities for the single events.

The final results for the calculation of $\mathcal{E}$ are given in Table V, where the contributions from each type of secondary are listed separately. The amount of uncertainty listed with each secondary includes the statistical uncertainty of the Monte-Carlo calculation, the effect of the uncertainty in the shape of the initial spectra used in the calculation, and an estimate of the systematic errors from the energy threshold determination and the calculated energy loss. In addition to these, two other effects are likely to have an important influence on the result: the effect of finite edges of the NaI crystals, and the scattering of particles from the walls of the lead shielding surrounding the crystals. The edge effect was estimated by comparing the solid angle subtended by the edges with that subtended by the entire crystal. This gave an estimated uncertainty of ±11%. An upper limit to the scattering from the walls of the lead shielding was estimated assuming isotropic scattering of all charged particles intercepting the walls. This gave a 4% increase to the total solid angle, so we have taken (2±2)% as an estimate of the increase in the efficiency from this effect. The fraction of gammas forming showers in the walls which give addisional counts in the crystals is expected to be negligible, tince the widths of the showers[44] are small.

TABLE V. A summary of the calculated efficiency for detecting stopping K^- by counting secondaries with the NaI detectors. The estimated uncertainty in the total value includes the uncertainty listed for each secondary plus estimates of edge effects in the detectors and scattering from the surrounding shielding (see text). The uncertainties have been combined in quadrature.

Type of secondary	Number detected per stopped K^-
γ	0.0105±0.0005
π^-(<49 MeV)	0.0104±0.0016
π^-(>49 MeV)	0.0225±0.0016
π^+	0.0047±0.0004
p	0.0060±0.0003
n	0.0012±0.0001
multiple	0.0077±0.0004
Total	0.0630±0.0076

PHYSICAL REVIEW VOLUME 158, NUMBER 5 25 JUNE 1967

Two-Prong + K_1^0 Events in K^-d Interactions at 2.24 BeV/c†

K. F. GALLOWAY, R. J. DEREMER,* E. D. ALYEA, JR., R. R. CRITTENDEN, H. J. MARTIN, JR., AND J. H. SCANDRETT‡
Indiana University, Bloomington, Indiana
(Received 13 January 1967)

A total of 702 events with two charged particles and a K_1^0 meson in the final state have been measured. Three hundred and eighty-five of these events represented the $K^-d \to \bar{K}^0\pi^- pn$ reaction and they have been divided, using the spectator model, into 247 $K^-p \to \bar{K}^0 p\pi^-$ events and 138 $K^-n \to \bar{K}^0\pi^- n$ events. Both reactions show resonance production. The $K^-p \to \bar{K}^0\pi^- p$ reaction has (56±5)% $K^{*-}p$ final state; the $K^-n \to \bar{K}^0\pi^- n$ reaction has equal N^{*-} and K^{*-} production, (26±8)% $K^{*-}n$ in the final state and (25±8)% $\bar{K}^0 N^{*-}$. Angular distributions and information on other final states are also given.

INTRODUCTION

THE work presented in this paper is part of a bubble-chamber study of K^- mesons interacting in deuterium at 2.24 BeV/c. The data include all events with two charged particles and a K_1^0 meson in the final state. This final state is dominated by the $K^-d \to \bar{K}^0\pi^- pn$ reaction and its experimental features are consistent with an impulse approximation model in which the incident beam interacts with only one of the nucleons in the deuteron. Results on the $K^-p \to \bar{K}^0\pi^- p$ and the $K^-n \to \bar{K}^0\pi^- n$ reactions have been extracted from the data and a comparison of these reactions is given.

Experimental studies of the $K^-p \to \bar{K}^0\pi^- p$ reaction at several beam energies show that the final state is dominated by the K^*(891 MeV) resonance and that the production and decay characteristics of this resonance are consistent with a production model involving one-meson exchange. Isospin considerations within the framework of this exchange model indicate that K^{*-} production in the K^-n and K^-p reactions should be similar. There are, of course, differences between the two reactions and variations from the isospin predictions are expected. The results that will be presented here, although limited by statistics, indicate differences

† Supported in part by the National Science Foundation.
* Current address: Physics Department, San Bernadino State College, San Bernadino, California.
‡ Current address: Department of Physics, Washington University, St. Louis, Missouri.

between the two reactions and a possible sensitivity of the one-meson-exchange model corrections to different isospin states.

I. EXPERIMENTAL PROCEDURES

The experiment was conducted at the Alternating Gradient Synchrotron (AGS) at Brookhaven National Laboratory. The BNL 20-in. bubble chamber (filled with deuterium) was exposed to a separated K^- beam with momentum 2.24 ± 0.02 BeV/c.[1] Approximately 100 000 pictures were taken with six to seven K^- tracks ($\sim$9-beam tracks) per picture. The photographs were scanned twice for (among other things) all two-prong-plus-vee events. These events were then measured on either an Itek Film Reader or a digitizer of the Adair-Leipuner design. Standard programs were used for the geometrical reconstruction and kinematic fitting.[2]

The vees were examined to separate the Λ^0 and K_1^0 production events. Selection was made on the basis of the kinematic fit to the vee and estimates of the track bubble densities. Association of the vees with the production vertex was also required. A total of 702 two-prong plus K_1^0 events satisfied these criteria. About 10% of these events had overlapping Λ^0 and K_1^0 vee fits and were selected as K_1^0 production events after examining the missing masses, track-bubble densities and χ^2 probabilities.

A $pn\bar{K}^0\pi^-$ final state was hypothesized and tested for all events. To be classified as a $pn\bar{K}^0\pi^-$ event, the track ionizations at the production vertex had to be consistent with this choice; the neutral missing mass had to be within three standard deviations of the neutron mass; and the fit was required to have a confidence level greater than 1% ($\chi^2\leq6.6$). Examination of track-bubble densities for the remaining events led to samples containing $\pi^+\pi^-K_1^0$+neutrals and $pK_1^0\pi^-$+neutrals. For the sample, $pK_1^0\pi^-$+neutrals, the neutral missing mass plus three standard deviations had to be greater than 1080 MeV. A similar lower bound at 1878 MeV was used for the sample $\pi^+\pi^-K_1^0$+neutrals. A small number of events fit the hypothesis $K^-d\rightarrow\bar{K}^0d\pi^-$ and a sample of this final state was selected. [See Sec. II F.] As a result of the above procedure, the two-prong plus K_1^0 events were divided as follows:

$K^-d\rightarrow pnK_1^0\pi^-$,	385 events;
$K^-d\rightarrow dK_1^0\pi^-$,	8 events;
$K^-d\rightarrow pK_1^0\pi^-$+neutrals,	185 events;
$K^-d\rightarrow\pi^+\pi^-K_1^0$+neutrals,	108 events.

With the above criteria, 16 events ($\sim$2%) failed to fit any category.

The categories are relatively pure. The background from pion contamination in the incident beam is less than 3%. No effort has been made to separate out events with multiple strange particles; for example, $K^-d\rightarrow K^0\pi^-p\Xi^0$ and $K^-d\rightarrow K^0K^-p\Lambda^0$ events. Background from these and similar reactions is less than 3%.

II. EXPERIMENTAL RESULTS

A. The Spectator Model

A spectator model has been assumed for the $K^-d\rightarrow\bar{K}^0\pi^-pn$ events. The validity of such a model has been established in a number of experiments.[3–5] The basic assumption is that the incident K^- interacts with only one of the two nucleons in the deuteron, and that the momentum distribution of the other (spectator) nucleon is given by the square of the Fourier transform of the Hulthén wave function[6] for the deuteron.

In this experiment, the lower momentum nucleon in each event is assumed to be the spectator particle in order to separate the K^-p and K^-n interactions. The spectator-nucleon momentum distribution for both reactions is shown in Fig. 1. The detection efficiency for observing protons in the bubble chamber decreases rapidly at lower momenta and accounts for the loss of protons below 75 MeV/c indicated in Fig. 1(b). A total of 71 spectator nucleons have momenta greater than 300 MeV/c. They are not predicted by the Hulthén distribution. There are also 33 events in which both nucleons have momenta less than 300 MeV/c. The events in these two categories do not bias the distributions presented in this paper and are included in the final samples. Under the assumption of a spectator model the sample of 385 $K^-d\rightarrow\bar{K}^0\pi^-pn$ events divides into 247 $K^-p\rightarrow\bar{K}^0\pi^-p$ events and 138 $K^-n\rightarrow\bar{K}^0\pi^-n$ events.

B. $K^-p\rightarrow\bar{K}^0\pi^-p$

Production of the K^* (891) resonance completely dominates this reaction. The $(\bar{K}^0\pi^-)$ effective mass plot is shown in Fig. 2(a). There is no enhancement in the $(\bar{K}^0p)$ state [Fig. 2(b)] and very little isobar production

[1] J. Leitner, G. Moneti, and N. P. Samios, Nucl. Instr. Methods **20**, 42 (1963).

[2] The reconstruction programs were modified versions of DATPRO programs kindly supplied to us by Dr. R. K. Adair, Dr. L. Leipuner, and Dr. B. Musgrave. The kinematic fitting program was the IOWA STATE FORTRAN GUTS program kindly supplied by Dr. W. J. Kernan.

[3] R. Kraemer, L. Madansky, M. Meer, M. Nussbaum, A. Pevsner, C. Richardson, R. Strand, R. Zdanis, T. Fields, S. Orenstein, and T. Toohig, Phys. Rev. **136**, B496 (1964).

[4] W. Chinowsky, G. Goldhaber, S. Goldhaber, W. Lee, T. O'Halloran, T. Stubbs, W. E. Slater, D. H. Stork, and H. K. Ticho, in *Proceedings of the Tenth Annual Rochester Conference on High-Energy Physics, 1960* (Interscience Publishers, Inc., New York, 1960), p. 451.

[5] I. Butterworth, J. Brown, G. Goldhaber, S. Goldhaber, A. Hirata, J. Kadyk, B. Schwarzschild, and G. Trilling, Phys. Rev. Letters **15**, 734 (1965).

[6] L. Hulthén and M. Sugawara, *Handbuch der Physik*, edited by S. Flügge (Springer-Verlag, Berlin, 1957), Vol. 39, p. 1.

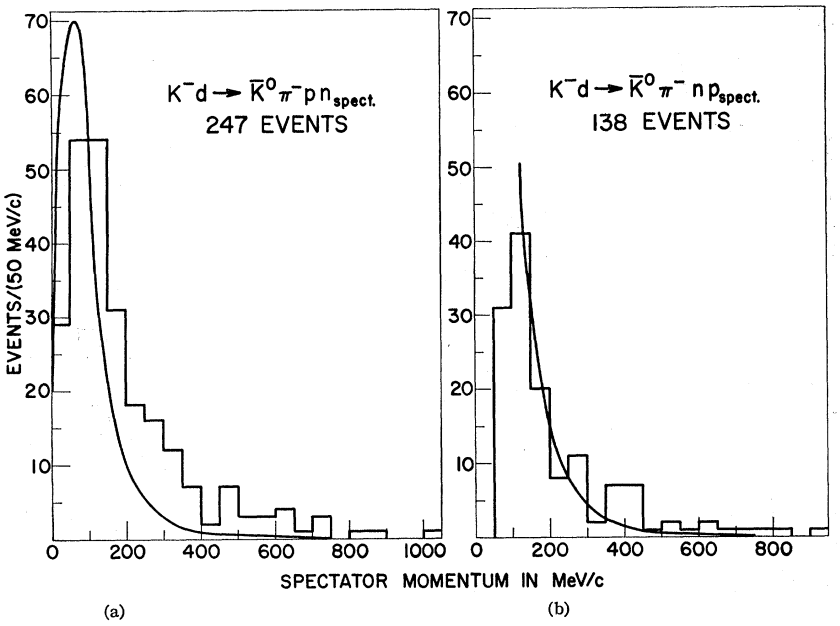

FIG. 1. (a) The momentum distribution for the neutrons in the reaction $K^-d \to \bar{K}^0\pi^- p n_{\text{spect.}}$. The Hulthén distribution is normalized to the number of events between 0 and 300 MeV/c. (b) The momentum distribution for the protons in the reaction $K^-d \to \bar{K}^0\pi^- n p_{\text{spect.}}$. The Hulthén distribution is normalized to the number of events between 100 and 300 MeV/c.

in the $(\pi^- p)$ state [Fig. 2(c)]. These three observations agree with $K^- p$ experiments at nearby energies.[7-9]

In order to estimate relative cross sections for K^{*-} and N^{*0} production, we have made a maximum-likelihood calculation using the Dalitz plot population and assuming that the resonant and background contributions to the $p\bar{K}^0\pi^-$ final state do not interfere. The masses and widths of the two resonances were fixed at their accepted values for the calculation. The resonant terms in the likelihood function had the form,[10,11] $D_R=[\Gamma_R/(\Gamma_R^2 M_R^2+(M_R^2-M_{12}^2)^2)](M_{12}q_3/p_1)$, where M_R and Γ_R are the mass and width of the resonance; M_{12} is the effective mass of particles 1 and 2, the decay particles of the resonance; p_1 is the momentum of particle 1 in the M_{12} rest frame; and q_3 is the momentum of M_{12} in the overall c.m. system. The width Γ_R is energy dependent and is given by Jackson[11] for the K^* and N^*.

The likelihood function

$$L(f_{K^*},f_{N^*})=(1-f_{K^*}-f_{N^*}) +(f_{K^*}D_{K^*}/A_{K^*})+(f_{N^*}D_{N^*}/A_{N^*}),$$

with f_R the fraction of events in which R is produced

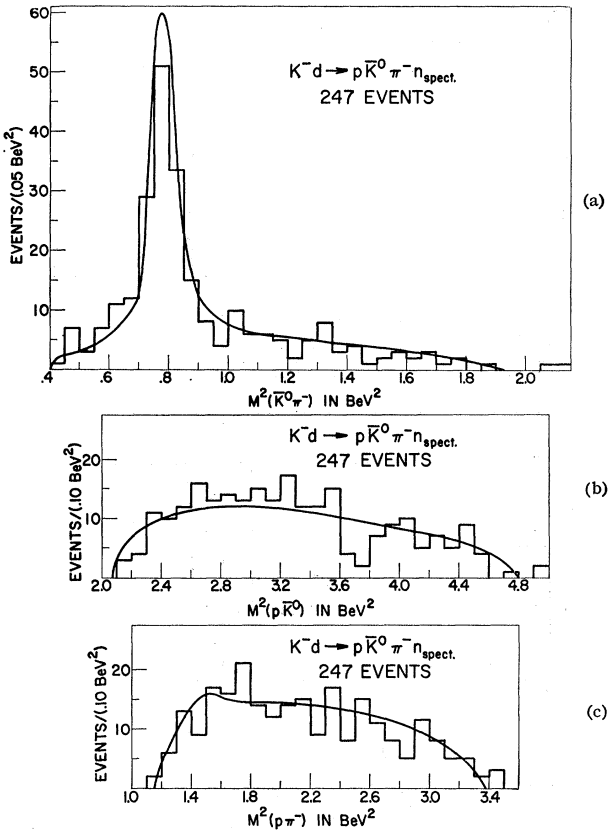

FIG. 2. The two-body effective mass combinations for the reaction $K^-p \to \bar{K}^0\pi^- p$. The solid curves in (a) and (c) represent the likelihood calculation and are discussed in the text. The solid curve in (b) is the phase-space curve.

[7] R. Barloutaud, A. Leveque, G. Louedec, J. Meyer, P. Schlein, A. Verglas, J. Badier, M. Demoulin, J. Goldberg, B. P. Gregory, P. Krejbich, C. Pelletier, M. Ville, E. S. Gelsema, J. Hoogland, J. C. Kluyver, and A. G. Tenner, Phys. Letters **12**, 352 (1964).

[8] G. W. London, R. R. Rau, N. P. Samios, S. S. Yamamoto, M. Goldberg, S. Lichtman, M. Primer, and J. Leitner, Phys. Rev. **143**, 1034 (1966).

[9] L. T. Smith, D. H. Stork, and H. K. Ticho, in *Proceedings of the Second Annual Athens Topical Conference on Resonant Particles* (Ohio University, Athens, Ohio, 1965), p. 380.

[10] M. Ferro-Luzzi, R. George, Y. Goldschmidt-Clermont, V. P. Henri, B. Jongejans, D. W. G. Leith, G. R. Lynch, F. Muller, and J. M. Perreau, Nuovo Cimento **36**, 1101 (1965).

[11] J. D. Jackson, Nuovo Cimento **34**, 1644 (1964).

and

$$A_R = \int D_R dM_{12}^2 dM_{23}^2 \Big/ \int dM_{12}^2 dM_{23}^2,$$

was maximized with the aid of STEPIT,[12] a subroutine for finding local minima. The results of the calculation gave $(5\pm2)\%N^{*0}$ and $(56\pm5)\%K^{*-}$ in the $\bar{K}^0\pi^- p$ final state. Due to the assumptions involved in this model, small amounts of resonance production cannot be accurately calculated. The N^{*0} production given by the likelihood fit should be regarded as a possible upper limit. The curves in Fig. 2 show the fit to the data.

The most striking feature of the production of the K^* is its peripherality. The momentum-transfer distribution is shown in Fig. 3(a).

Some understanding of the production mechanism can be derived from a study of the resonance decay distributions. The distributions for the $\bar{K}^0$ from the decay of the K^* are[13]

$$W_{K^*}(\cos\theta)d\cos\theta = \tfrac{3}{4}[(1-\rho_{0,0})+(3\rho_{0,0}-1)\cos^2\theta]d\cos\theta,$$

$$W_{K^*}(\varphi)d\varphi = \frac{1}{2\pi}[1-2\rho_{1,-1}+4\rho_{1,-1}\sin^2\varphi]d\varphi,$$

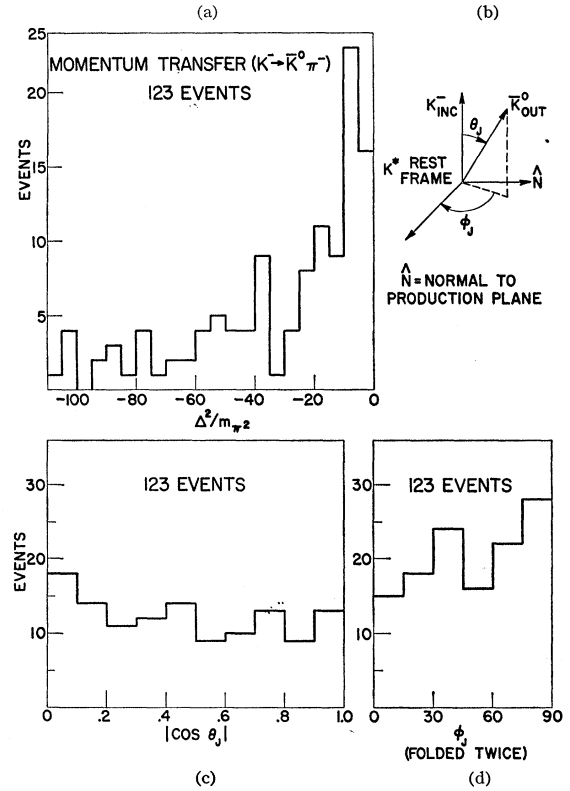

FIG. 3. Momentum transfer and decay correlations for the K^*- produced in the reaction $K^- p \to \bar{K}^0\pi^- p$. The events are chosen such that 0.84 BeV $\leq M_{\bar{K}^0\pi^-} \leq$ 0.94 BeV. The coordinate system defining the decay correlations is given in (b).

[12] STEPIT by J. P. Chandler, distributed by Quantum Chemistry Program Exchange, Department of Chemistry, Indiana University.

[13] K. Gottfried and J. D. Jackson, Phys. Letters 8, 144 (1964); Nuovo Cimento 33, 309 (1964).

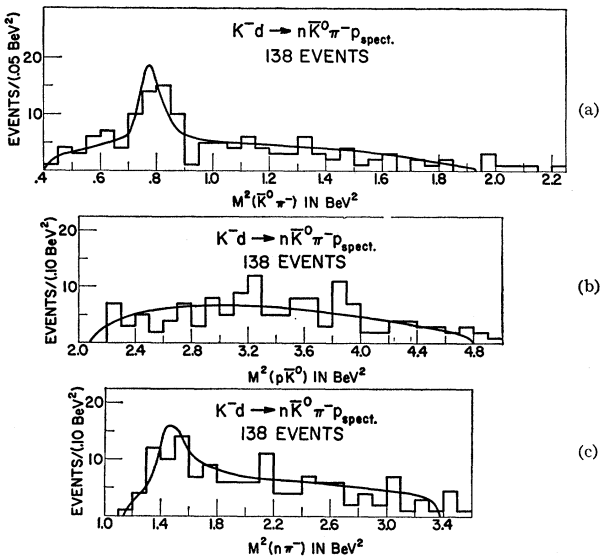

FIG. 4. The two-body effective mass combinations for the reaction $K^- n \to \bar{K}^0\pi^- n$. The solid curves in (a) and (c) represent the likelihood calculation and are discussed in the text. The solid curve in (b) is the phase-space curve.

where θ and φ are the polar and azimuthal angles in the rest frame of the K^* as defined in Fig. 3(b) and $\rho_{0,0}$, $\rho_{1,-1}$ are elements of the spin-space density matrix of the K^*. These distributions assume that the K^* is a freely decaying particle with spin 1. The experimental

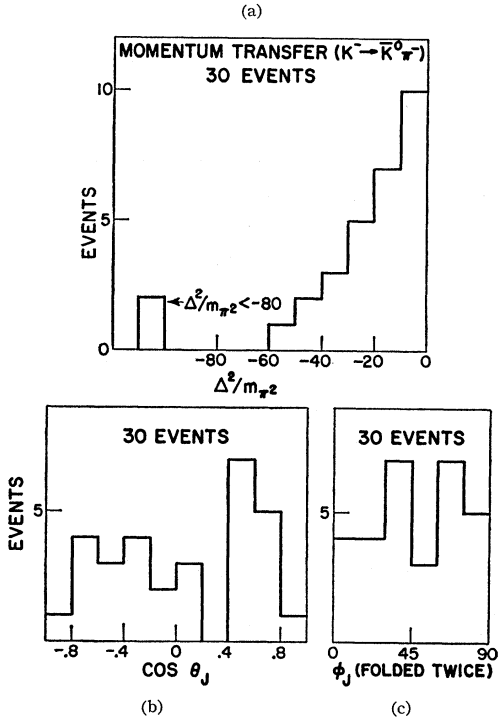

FIG. 5. Momentum transfer and decay correlations for the K^{*-} produced in the reaction $K^- n \to \bar{K}^0\pi^- n$. The events are chosen such that 0.84 BeV $\leq M_{\bar{K}^0\pi^-} \leq$ 0.94 BeV. Events that also lie in the N^{*-} band have been removed (1116 MeV $\leq M_{n\pi^-} \leq$ 1356 MeV).

distributions are shown in Figs. 3(c) and 3(d) for events with $(\bar{K}^0\pi^-)$ effective masses between 0.84 and 0.94 BeV. The parameter $\rho_{0,0}$ can be interpreted as the fraction of the events that are produced by pion exchange. A maximum-likelihood fit to the data gives $\rho_{0,0}=0.43\pm0.05$.

C. $K^-n\rightarrow\bar{K}^0\pi^-n$

About one-half of the time, this reaction proceeds through one of the two body final states, $N^{*-}\bar{K}^0$ or $K^{*-}n$. Production of these resonances can be seen in the effective-mass plots shown in Fig. 4. A maximum-likelihood fit to these data gives $(26\pm8)\%K^{*-}n$ production and $(25\pm8)\%\bar{K}^0N^{*-}$ production. The curves in Fig. 4 compare this fit with the data.

The momentum-transfer distribution for K^{*-} production is shown in Fig. 5(a). The events are chosen such that the $(\bar{K}^0\pi^-)$ effective masses lie between 0.84 and 0.94 BeV. Events that also lie in the N^{*-} band (1116 MeV$\leq M_{n\pi^-}\leq$1356 MeV) have been removed from the distributions in Fig. 5. Once again, the peripheral nature of the K^* production is apparent. The distributions in θ and φ for the K^{*-} decay are shown in Figs. 5(b) and 5(c). A fit to these data gives $\rho_{0,0}=0.21\pm0.08$.

Similar curves for the N^{*-} production are shown in Fig. 6, with the K^{*-} events removed. The mass cuts used here are the same as in the preceding paragraph. One unexpected feature is that the N^{*-} momentum-transfer distribution appears to be somewhat narrower than the K^{*-} distribution. The one-meson-exchange model requires vector-meson exchange in the N^{*-} production and the narrow width is not expected.

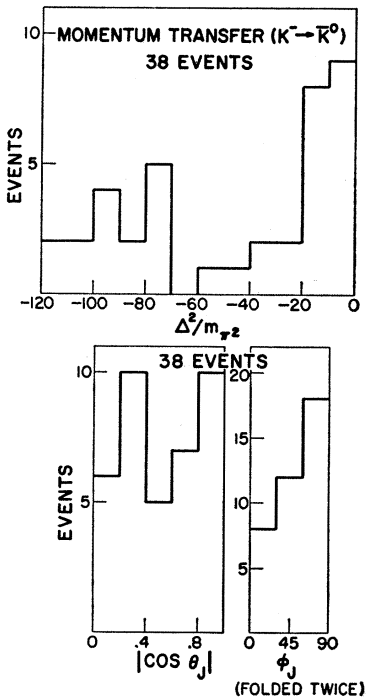

FIG. 6. Momentum transfer and decay correlations for the N^{*-} produced in the reaction $K^-n\rightarrow\bar{K}^0\pi^-n$. The events are chosen such that 1116 MeV$\leq M_{n\pi^-}\leq$1356 MeV. Events that also lie in the K^{*-} band have been removed (0.84 BeV $\leq M_{\bar{K}^0\pi^-}\leq$0.94 BeV).

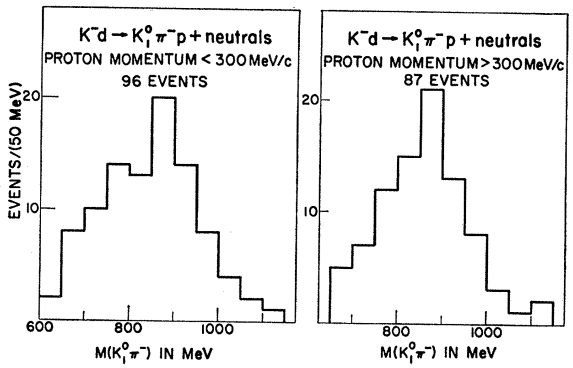

FIG. 7. The effective mass distribution for $(K_1^0\pi^-)$ produced in the reaction $K^-d\rightarrow K_1^0\pi^-p+$neutrals. The events have been divided into two groups on the basis of proton momentum: one with the proton momentum less than 300 MeV/c and the other with the proton momentum greater than 300 MeV/c.

D. $K^-d\rightarrow pK_1^0\pi^-+$Neutrals

The positive track in these events was classified as a proton using bubble-density estimates. The neutral missing mass plus three standard deviations was also required to be greater than 1080 MeV. The data can be divided, in keeping with the spectator model, by separately grouping events with proton momentum greater than 300 MeV/c and events with proton momentum less than 300 MeV/c. The $(K_1^0\pi^-)$ effective mass plots for both groups are shown in Fig. 7. Production of the K^{*-} is evident in both plots.

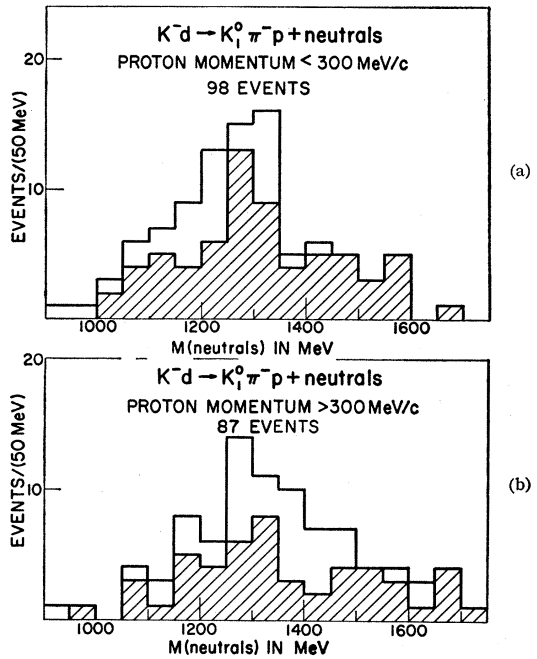

FIG. 8. The effective mass distribution for the neutrals in the reaction $K^-d\rightarrow K_1^0\pi^-p+$neutrals. The shaded area represents events with the $(K_1^0\pi^-)$ mass outside the K^* region, which is defined to lie between the limits 0.84 BeV$\leq M_K\leq$0.94 BeV. The events have been divided into two groups on the basis of proton momentum: one with the proton momentum less than 300 MeV/c and the other with the proton momentum greater than 300 MeV/c.

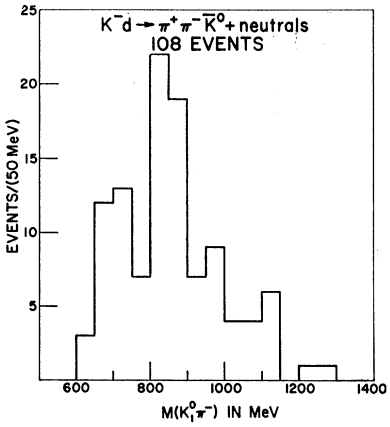

FIG. 9. The effective mass distributions for $(K_1^0\pi^-)$ in the reaction $K^-d \to K_1^0\pi^-\pi^+$+neutrals.

The neutral missing-mass spectra for both groups are shown in Fig. 8. The shaded histograms contain events in which the $(K_1^0\pi^-)$ effective mass lies outside the K^*-mass region.

While the cut on proton momentum shows no effect in the $(K_1^0\pi^-)$ mass plots, this cut with the requirement that the $(K_1^0\pi^-)$ mass lie outside the K^* region, which is defined by the limits 0.84 BeV$\leq M_{K\pi} \leq$0.94 BeV, shows some evidence for the $K^-d \to p_{\text{spect}}K_1^0\pi^-\Xi^0$ reaction [see Fig. 8(a)].

E. $K^-d \to \pi^+\pi^-K_1^0$+Neutrals

The $(K_1^0\pi^-)$ effective mass distribution for these events is shown in Fig. 9. There is evidence for K^{*-} production.

F. $K^-d \to \bar{K}^0\pi^-d$

A total of 41 events had kinematic fits to this reaction. All of these events also fit the $K^-d \to K_1^0\pi^-pn$ reaction and the following criteria were imposed to select deuteron events: (1) the missing mass recoiling against the $(K_1^0\pi^-)$ system in the final state had to be within three standard deviations of the deuteron mass; (2) the neutral missing mass, assuming a $\bar{K}^0\pi^-d$ final state, had to be within three standard deviations of zero; and (3) the χ^2 probability for the $\bar{K}^0\pi^-d$ final state had to be greater than the χ^2 probability for the $\bar{K}^0\pi^-pn$ final state. Eight acceptable events were found. Seven of these eight events have $(\bar{K}^0\pi^-)$ effective masses near the mass of the K^{*-} resonance. The mass plots are not presented because of the limited statistics.

G. Cross Sections

A total kaon path length of 17×10^6 cm. was examined for two-prong plus K_1^0 events. The total yield was 0.66 events per microbarn. Several corrections had to be made. The charged-decay mode of the K_1^0 meson occurs one-third of the time when a $\bar{K}^0$ or K^0 is produced. A correction must also be made for the experimental detection efficiency of the charged K_1^0 decay. The average value of the detection efficiency is 0.85. Two other corrections arise when the incident kaon is assumed to interact with a single nucleon. A Glauber correction of 7% allows for the screening of one nucleon by the other. The final correction uses the Hulthén momentum distribution for the proton in the deuteron and gives an estimated efficiency of 0.43 for detecting spectator protons. The cross sections are given in Table I.

TABLE I. Cross sections for final states identified.

Reaction	Events	Cross section (μb)
$K^-p \to K_1^0\pi^-p$	247	1435±277
$K^-n \to K_1^0\pi^-n$	138	1869±388
$K^-d \to pK_1^0\pi^-$+neutrals	185	995±198[a]
$K^-d \to \pi^-\pi^+K_1^0$+neutrals	108	581±125[a]
$K^-d \to K_1^0\pi^-d$	8	43±17[b]

[a] Cross sections have not been corrected for undetected spectators.
[b] No correction has been made for undetected deuterons.

III. DISCUSSION

Our data on the $K^-p \to \bar{K}^0\pi^-p$ reaction are in good agreement with the results of a K^-p experiment at 2.24 BeV/c reported by London, *et al.*[8] They find peripheral production of the K^* resonance and very little evidence for the N^* resonance in the final state. Similar results are reported in this paper. The cross section reported here for the $K^-p \to \bar{K}^0\pi^-p$ reaction is also in agreement with the value reported by London.

If the K^{*-} production is described by a one-meson-exchange model, then its production cross section and other production characteristics should be the same in the K^-p and K^-n reactions. Interference effects in the two reactions may differ if both isoscalar and isovector meson exchange occurs. Absorption corrections to the model may also be different for the two reactions.

Experimentally, K^* production appears to be inhibited in the K^-n reaction. We find $\sigma(K^-n \to K^{*-}n)/\sigma(K^-p \to K^{*-}p)=0.6\pm0.1$. The other difference between the two reactions is the strong production of the N^{*-} resonance in the K^-n reaction. Interference effects between K^* and N^* resonances have been observed in the $K^+p \to K^0\pi^+p$ reaction.[14] Similar effects in this experiment might preclude comparison of the K^-p and K^-n reactions.

ACKNOWLEDGMENTS

We would like to express our gratitude to our scanning and measuring staff and to Brookhaven National Laboratory and the Alternating Gradient Synchroton (AGS) operating staff for their aid during this exposure.

[14] R. W. Bland, M. G. Bowler, J. L. Brown, G. Goldhaber, S. Goldhaber, J. A. Kadyk, and G. H. Trilling, Phys. Rev. Letters 17, 939 (1966).